Available online at www.sciencedirect.com
SCIENCE DIRECT®
ELSEVIER
International Journal of Solids and Structures 42 (2005) 6122–6140
INTERNATIONAL JOURNAL OF SOLIDS and STRUCTURES
www.elsevier.com/locate/ijsolstr

Dynamic analysis of composite plate with multiple delaminations based on higher-order zigzag theory

Jinho Oh [a], Maenghyo Cho [a,*], Jun-Sik Kim [b]

[a] *School of Mechanical and Aerospace Engineering, Seoul National University, San 56-1, Shillim-Dong, Kwanak-Gu, Seoul 151-744, Republic of Korea*
[b] *Department of Aerospace Engineering, The Pennsylvania State University, University Park, PA 16802, United States*

Received 17 May 2004; received in revised form 31 May 2005
Available online 20 July 2005

Abstract

In a recent paper, Cho and Kim [Journal of Applied Mechanics] proposed a higher-order cubic zigzag theory of laminated composites with multiple delaminations. The proposed theory is not only accurate but also efficient because it work with a minimal number of degrees of freedom with the application of interface continuity conditions as well as bounding surface conditions of transverse shear stresses including delaminated interfaces. In this work, we investigate the dynamic behavior of laminated composite plates with multiple delaminations. A four-node finite element based on the efficient higher-order zigzag plate theory of laminated composite plates with multiple delaminations is developed to refine the prediction of frequencies, mode shape, and time response. Through the dynamic version of the variational approach, the dynamic equilibrium equations and variationally consistent boundary conditions are obtained. Natural frequency prediction and time response analysis of a composite plate with multiple delaminations demonstrate the accuracy and efficiency of the present finite element method. To prevent penetration violation at the delamination interfaces, unilateral contact constraints by Lagrange multiplier method are applied in the time response analysis. The present finite element is suitable for the prediction of dynamic response of thick composite plates with multiple and arbitrary shaped delaminations.

Keywords: Multiple delaminations; Zigzag theory; Time integration; Finite element; Unilateral contact; Lagrange multiplier; Natural frequency; Mode shape

* Corresponding author. Tel.: +82 2 880 1695; fax: +82 2 886 1693.
E-mail address: mhcho@snu.ac.kr (M. Cho).

0020-7683/$ - see front matter © 2005 Elsevier Ltd. All rights reserved.
doi:10.1016/j.ijsolstr.2005.06.006

1. Introduction

Recently, many researchers have given special attention to the development of advanced composite materials because they possess high specific strength and stiffness which are advantageous in the applications of aircraft, marine, and automobiles. In particular, analysis of dynamic characteristics is quite important to understand the stability and strength of structures. Especially for structural design in the critical environments, highly accurate dynamic analysis is required. For the enhanced analysis of laminated composite plates, three types of higher-order theory have been developed: the smeared theory (Lo et al., 1977), layerwise theory (Reddy, 1987), and simplified zigzag theory (Di Sciuva, 1986). Extensive up-to-date reviews can be found in the review papers of Noor and Burton (1989), Kapania and Raciti (1989), and Reddy and Robbins (1994). Recently, the so-called "zigzag" theories in the third category have received much attention because of their accuracy and efficiency in the ply-level analysis. Most of the theories assume that interfaces are perfectly bonded (Di Sciuva, 1986; Cho and Parmerter, 1992, 1993). A postprocess method based on zigzag theory was also proposed (Cho and Kim, 1996). However, in many applications, this assumption is not adequate for the prediction of the behaviors of composite laminates. Low-speed impacts by foreign objects or imperfections in the manufacturing process may generate multiple delaminations in composite laminates. Strength and stiffness of composite structures with delaminations decrease more significantly than the undelaminated composite plates.

Therefore, vibration problems of delaminated beam/plate have been analyzed by numerous researchers. The classical beam model (Wang et al., 1982; Wang and Lin, 1995), first-order shear deformation model (Shen and Grady, 1992; Gummadi and Hanagud, 1995), and higher-order shear model with piezolayers (Chattopadhyay et al., 1999; Seeley and Chattopadhyay, 1999) were employed for the natural frequency analysis. Damage detection/health monitoring problems were also considered in the frameworks of vibration analysis (Islam and Craig, 1994).

For the analysis of multi-layered laminated plates with arbitrary shaped multiple delaminations, finite element method is a suitable choice to treat the general loading, boundary conditions, layups, and geometry. Even though finite element based on layerwise plate theory (Lee et al., 1993) can provide an adequate framework for the delamination analysis, this theory is not computationally efficient since the number of degrees-of-freedom of this theory depends upon the number of layers. Thus, to reduce the active degrees-of-freedom of the problem, a global–local approach has been proposed by Cho and Kim (1997), Cho and Lee (1998), and Kim and Cho (1999).

In the recent study, zigzag higher-order theories have been extended to the weakened interface problem (Cheng et al., 1996; Di Sciuva, 1997). But the zigzag theory, which describes the opening as well as slipping behavior of the delaminated parts, has not appeared until Cho and Kim (2001) present an efficient higher-order laminated plate theory with delaminations. Chattopadhyay and Gu (1994) developed a higher-order theory to analyze the delamination buckling problem. However, this theory is complicated and employs many primary variables. An efficient higher-order zigzag theory with minimal degrees-of-freedom was developed to analyze multiple delamination problem (Cho and Kim, 2001). Buckling and vibration of one-dimensional beam-plate were analyzed in Cho and Kim (2001). The bifurcation buckling of two-dimensional plate with multiple delaminations was reported in Kim and Cho (2002). The buckling of shells with multiple-delaminations based on the same model was presented in Kim and Cho (2003).

In the present study, we focus on the dynamic behaviors of composite laminated plates with arbitrary multiple delaminations. Eigenvalue problems and time responses are analyzed. In the early stage of dynamic analysis, The finite element method for contact-impact problem was developed by Thomas et al. (1976). Ramkumar et al. (1983) proposed composite beam modeling technique with delamination. Especially, Shen and Grady (1992) experimented for a beam with rectangular delamination to obtain first opening mode shape. Dynamic model for laminated plates with a delamination was performed by Todd and

Frank (1998). The analysis of composite plate under dynamic loading which is induced by low velocity impacts was reported in Sekine et al. (1998).

The model in the present study is based on the efficient higher-order zigzag plate theory with minimal degrees of freedom which was proposed in the previous papers (Cho and Kim, 2001; Kim and Cho, 2002). Especially, in the analysis of time response of delaminated plate, the violation of unilateral contact conditions in the delaminated region is prohibited by imposing contact constraints through the Lagrange multipliers. The natural frequencies and time responses obtained from the present study are compared to those of the previously reported results (Shen and Grady, 1992; Chattopadhyay et al., 2000). The developed finite element was numerically verified by using laminated composites with circular, elliptic, and rectangular shaped delaminations, respectively. The present finite element method is suitable in the predictions of the dynamic response of a thick composite plate with multiple and arbitrary delaminations.

2. Displacement model

In this section, a higher-order zigzag displacement field for composite plates with multiple delaminations is briefly reviewed. The detailed description can be found in the previous works (Cho and Kim, 2001; Kim and Cho, 2002).

Displacement field of composite plates with multiple delaminations is considered. The deformation behavior is assumed within the range of linear elasticity. The configuration of the composite plate with multiple delaminations is shown in Fig. 1. Higher-order zigzag in-plane displacement field with delaminations is obtained by superimposing a zigzag linear field and piecewise constant delamination field to the globally cubic varying field.

The starting displacement field can be written as follows:

$$u_\alpha(x_\beta,z) = u_\alpha^0(x_\beta) + \psi_\alpha(x_\beta)z + \xi_\alpha(x_\beta)z^2 + \phi_\alpha(x_\beta)z^3 + \sum_{k=1}^{N-1} S_\alpha^k(x_\beta)(z-z_k)H(z-z_k) + \sum_{d=1}^{D} \bar{u}_\alpha^{\mathrm{d}}(x_\beta)H(z-z_d), \tag{1}$$

$$u_3(x_\beta,z) = w(x_\beta) + \sum_{d=1}^{D} \bar{w}^{\mathrm{d}}(x_\beta)H(z-z_d), \tag{2}$$

where u_α^0, w denote the displacement of a point on the reference plane. ψ_α are the rotations of the normal to the reference plane about the x_α axis. N is the number of total layers. D is the number of the delamination interfaces. $H(z-z_k)$ is the Heaviside unit step function. The terms $\bar{u}_\alpha^{\mathrm{d}}$, $\bar{w}^{\mathrm{d}}$ represent the possible jumps in the slipping and opening displacements, which permit the incorporation of the delamination for the laminated composites.

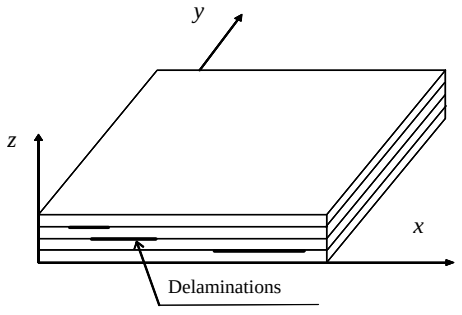

Fig. 1. Configuration of laminated composite plate with multiple delaminations.

The deformed schematic configuration and the kinematical variables are shown in Fig. 2. By applying top and bottom surface transverse shear stress free conditions, the following displacement field is obtained:

$$u_\alpha = u_\alpha^0 - w_{,\alpha} z - \Lambda_{\alpha\beta}\phi_\beta z^2 + \phi_\alpha z^3 + \sum_{k=1}^{N-1} S_\alpha^k(x_\beta)(z - z_k)H(z - z_k) + \sum_{d=1}^{D} \bar{u}_\alpha^{\mathrm{d}}(x_\beta)H(z - z_d), \tag{3}$$

$$u_3(x_\beta, z) = w(x_\beta) + \sum_{d=1}^{D} \bar{w}^{\mathrm{d}}(x_\beta)H(z - z_d), \tag{4}$$

in which,

$$\Lambda_{\alpha\beta} = \frac{3h}{2}\delta_{\alpha\beta} + \frac{1}{2h}\sum_{k=1}^{N-1} a_{\alpha\beta}^k. \tag{5}$$

Applying transverse shear stress continuity conditions at the interfaces between layers, the change of slope S_α^k can be determined in terms of the primary variables of reference plane:

$$S_\alpha^k = a_{\alpha\gamma}^k \phi_\gamma - \bar{w}_{,\alpha}^k \delta_{kd}, \tag{6}$$

where the coefficient $a_{\alpha\gamma}^k$ represents the change in the slope at each interface, and depend only upon the material properties of each layer. δ_{kd} is the Kronecker delta function. The term $\bar{w}_{,\alpha}^k \delta_{kd}$ represents the change in the slope at each delamination interface in which if the delamination terms $\bar{u}_\alpha^{\mathrm{d}}$ and $\bar{w}^{\mathrm{d}}$ are neglected, the displacement field is the same as that proposed by Cho and Parmerter (1992, 1993).

The strain tensor associated with the small displacement theory of elasticity are given by

$$\begin{aligned}\varepsilon_{\alpha\beta} &= \frac{1}{2}(u_{\alpha,\beta} + u_{\beta,\alpha}) \\ &= \frac{1}{2}\Bigg\{ u_{\alpha,\beta}^0 + u_{\beta,\alpha}^0 - (w_{,\alpha\beta} + w_{,\beta\alpha})z - \frac{3}{2}h(\phi_{\alpha,\beta} + \phi_{\beta,\alpha})z^2 - \frac{1}{2h}\sum_{k=1}^{N-1}(a_{\alpha\gamma}^k\phi_{\gamma,\beta} + a_{\beta\omega}^k\phi_{\omega,\alpha})z^2 + (\phi_{\alpha,\beta} + \phi_{\beta,\alpha})z^3 \\ &\quad + \sum_{k=1}^{N-1}(a_{\alpha\gamma}^k\phi_{\gamma,\beta} + a_{\beta\omega}^k\phi_{\omega,\alpha} - 2\bar{w}_{,\alpha\beta}^k\delta_{kd})(z - z_k)H(z - z_k) + \sum_{d=1}^{D}(\bar{u}_{\alpha,\beta}^{\mathrm{d}} + \bar{u}_{\beta,\alpha}^{\mathrm{d}})H(z - z_k)\Bigg\}\end{aligned} \tag{7}$$

$$\gamma_{\alpha 3} = u_{\alpha,3} + u_{3,\alpha} = -\left(3h\phi_\alpha + \frac{1}{h}\sum_{k=1}^{N-1} a_{\alpha\gamma}^k\phi_\gamma\right)z + 3\phi_\alpha z^2 + \sum_{k=1}^{N-1} a_{\alpha\gamma}^k\phi_\gamma. \tag{8}$$

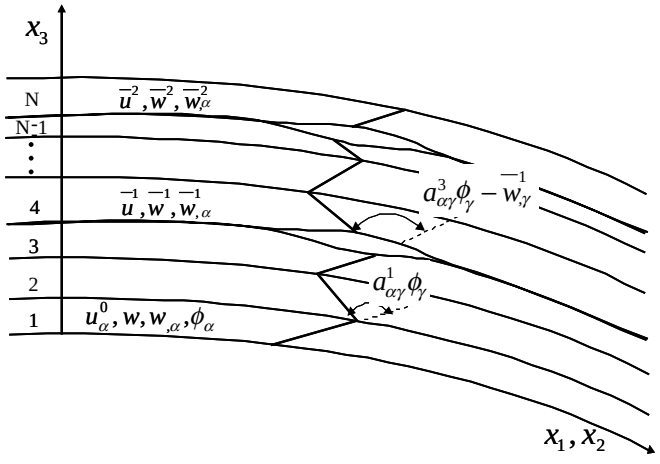

Fig. 2. Deformed configuration of laminates with multiple delaminations.

The equilibrium equations and boundary conditions can be derived from Hamilton principle and they can omitted here.

3. Finite element formulation

3.1. Stiffness matrix formulation

To assess the validity of the dynamic version of EHOPTWD (efficient higher-order plate theory with delamination; Cho and Kim, 2001; Kim and Cho, 2002), a finite element was developed for two-dimensional problems. The present laminated plate theory, which have been developed, has a second derivative of w (transverse deflection at the reference plane). Thus C^1 (slope-continuous) functions are required. However, it is well known in plate theory that it is difficult to impose C^1 conditions at the interfaces between elements in arbitrarily oriented quadrilateral and triangular elements. The triangular non-conforming element was developed by Specht (1988) and the rectangular non-conforming element was developed by Wanji and Cheung (1997). But, the DKQ element developed by Batoz and Tahar (1982) is the simplest element, which passes the patch test and satisfies the Kirchhoff constraints. In the present study, we adopted the concept of DKQ element to overcome the C^1 continuity problem.

The total potential energy can be divided into bending (including membrane term) and shear parts and unilateral Lagrange multiplier parts, which are needed to prevent penetration violations. Potential energy with Lagrange multiplier prohibits the penetration of the upper layer into the substrate layer at the delamination interfaces. The in-plane bending energy including the membrane energy $U_{\mathrm{b}}^{\mathrm{e}}$ and the transverse shear energy $U_{\mathrm{s}}^{\mathrm{e}}$ and unilateral constraint Lagrange multiplier U_{s}^{D} per element are expressed as

$$\Pi = U_{\mathrm{b}} + U_{\mathrm{s}} + U_{\mathrm{s}}^{D}, \tag{9}$$

where

$$\begin{aligned}
U_{\mathrm{b}}^{\mathrm{e}} &= \frac{1}{2}\int_{A^{\mathrm{e}}}\int_{0}^{h}\{\varepsilon\}^{\mathrm{T}}[Q_{\mathrm{b}}]^{(k)}\{\varepsilon\}\,\mathrm{d}z\,\mathrm{d}A^{\mathrm{e}} = \int_{A^{\mathrm{e}}}\{\varepsilon\}^{\mathrm{T}}[A_{\mathrm{b}}]\{\varepsilon\}\,\mathrm{d}A^{\mathrm{e}},\\
U_{\mathrm{s}}^{\mathrm{e}} &= \frac{1}{2}\int_{A^{\mathrm{e}}}\int_{0}^{h}\{\gamma\}^{\mathrm{T}}[Q_{\mathrm{s}}]^{(k)}\{\gamma\}\,\mathrm{d}z\,\mathrm{d}A^{\mathrm{e}} = \int_{A^{\mathrm{e}}}\{\gamma\}^{\mathrm{T}}[A_{\mathrm{s}}]\{\gamma\}\,\mathrm{d}A^{\mathrm{e}},\\
U_{\mathrm{s}}^{D} &= \begin{cases} 0 & \bar{w}^{\mathrm{d}} > 0,\\ \sum_{d=1}^{D}\lambda\bar{w}^{\mathrm{d}} & \bar{w}^{\mathrm{d}} < 0, \end{cases}
\end{aligned} \tag{10}$$

where, $[A_{\mathrm{b}}]$ and $[A_{\mathrm{s}}]$ are the stiffnesses of the bending and shear energies analytically integrated through the thickness to save the computing time, respectively. D is the node number of the delamination domain and λ is the Lagrange multiplier. The model configuration that considers the delamination contact by using Lagrange multiplier is shown in Fig. 3.

For the four-noded quadrilateral element, nodal displacement vector $\{a\}^{\mathrm{e}}$ is given by

$$\{a\}^{\mathrm{e}} = \left[u_{\alpha}^{0}, w, w_{,\alpha}, \phi_{\alpha}, \bar{u}_{\alpha}^{\mathrm{d}}, \bar{w}^{\mathrm{d}}, \bar{w}_{,\alpha}^{\mathrm{d}}\right]^{\mathrm{T}}. \tag{11}$$

Natural coordinates ξ and η are used in the shape functions and coordinate transformation functions.

The primary displacement unknowns are expressed in terms of nodal variables and shape functions as

$$u_{\alpha}^{0} = \sum_{i=1}^{4} N_i u_{\alpha i}^{0}, \qquad \bar{u}_{\alpha}^{\mathrm{d}} = \sum_{i=1}^{4} N_i \bar{u}_{\alpha i}^{\mathrm{d}}, \qquad \phi_{\alpha} = \sum_{i=1}^{4} N_i \phi_{\alpha i}, \tag{12}$$

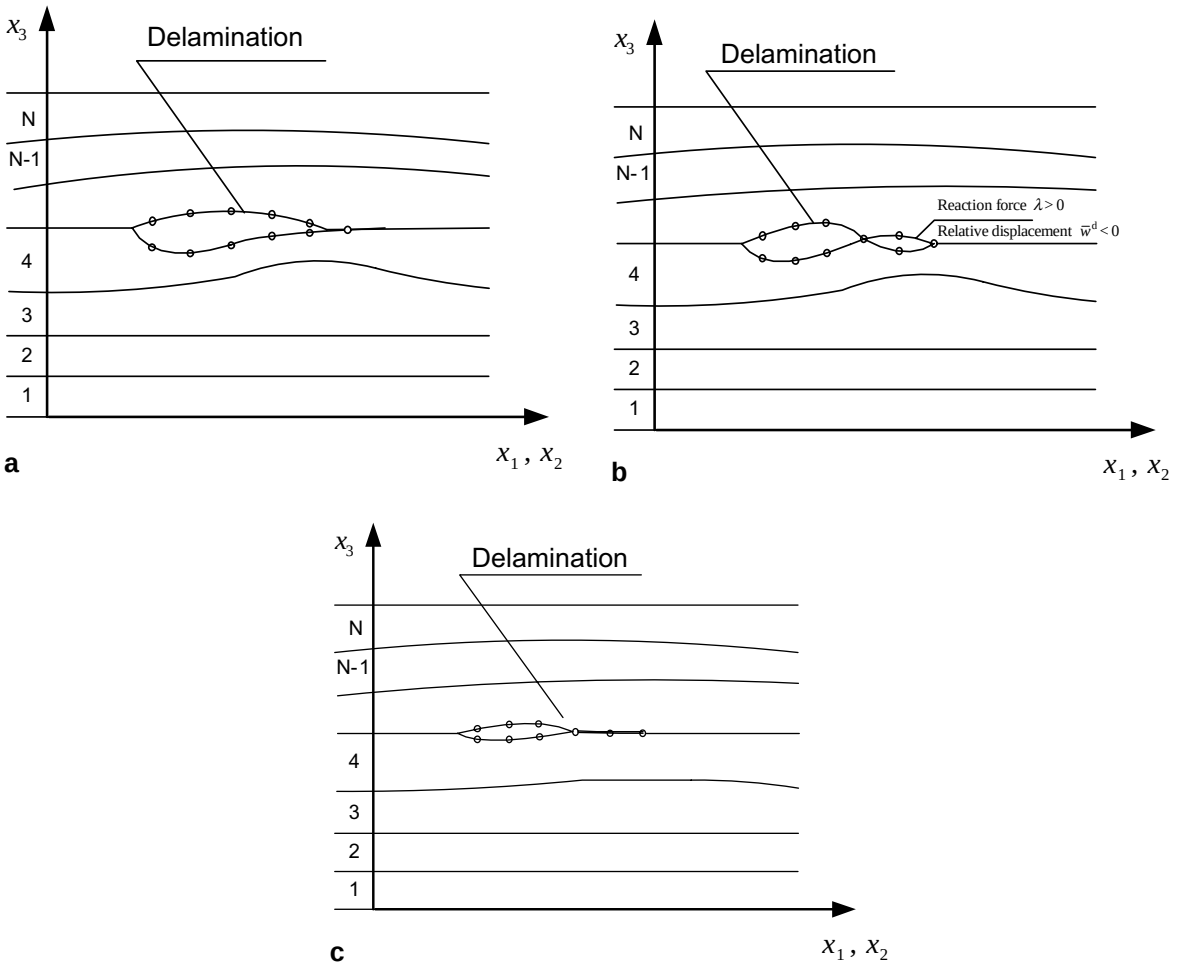

Fig. 3. Model configuration considering delamination contact by using Lagrange multiplier.

$$w_{,\alpha} = \sum_{i=1}^{4} \left\{ N_{\alpha i} w_i + P_{\alpha i} w_{,xi} + H_{\alpha i} w_{,yi} \right\}, \tag{13}$$

$$\bar{w}^{\mathrm{d}}_{,\alpha} = \sum_{i=1}^{4} \left\{ N_{\alpha i} \bar{w}^{\mathrm{d}}_i + P_{\alpha i} \bar{w}^{\mathrm{d}}_{,xi} + H_{\alpha i} \bar{w}^{\mathrm{d}}_{,yi} \right\}, \tag{14}$$

where N_i are the conventional bilinear shape functions, and $N_{\alpha i}$, $P_{\alpha i}$, and $H_{\alpha i}$ are the shape functions of the DKQ element.

3.2. Mass matrix formulation

In solving the eigenvalue problem and time integration analysis by the finite element method, a mass matrix is required. The eigenvalue problem is given as,

$$(K^{\mathrm{e}} - \omega^2 M^{\mathrm{e}})\{a\}^{\mathrm{e}} = \{0\}, \tag{15}$$

where K^e and M^e denote the element stiffness matrix and mass matrix, respectively, ω represents the natural frequency and $\{a\}^e$ indicates the eigen-vectors of nodal displacement corresponding to the eigenvalue.

However, the DKQ element cannot define the transverse deflection w inside an element. It only specifies w along the edge of the element. When a mass matrix is required, the transverse deflection w needs to be described within an element. Therefore, to compute the element mass matrix, a refined non-conforming displacement proposed by Cheung et al. (2000) is adopted.

The mass matrix in the element local system can be expressed as

$$M^e = \int_{V_e} \rho [N]^T [N] \, dV.$$

Refined non-conforming displacement w (Cheung et al., 2000) can be expressed as

$$w = w^* - \alpha(w^* - w_b) = N\{a\}, \tag{16}$$

$$w_b = \sum_{i=1}^{4} N_i w_i = N_b\{a\}, \tag{17}$$

where, w^* is the displacement function of 12-DOF quadrilateral element based on the non-conforming displacement, and w_b is a linear function. $\{a\}$ is nodal displacement vector and α is an adjustable constant.

Finally, we can obtain the following interpolation function for transverse deflection w:

$$N = N^* - \alpha(N^* - N_b), \tag{18}$$

$$w = \sum_{i=1}^{4} N_{wi} w_i + P_{wi} w_{,xi} + H_{wi} w_{,yi}. \tag{19}$$

In the delaminated zone, nodal displacement $\bar{w}^d$ can also be interpolated by the same subparametric function and it can be expressed as,

$$\bar{w}^d = \sum_{i=1}^{4} N_{wi} \bar{w}_i^d + P_{wi} \bar{w}_{,xi}^d + H_{wi} \bar{w}_{,yi}^d. \tag{20}$$

The explicit form of shape function $[N]$ used in constructing element mass matrix is given by,

$$[N] = \begin{bmatrix} B_1 & B_5 & [0]_{3\cdot 2} & [0]_{3\cdot 2d} & [0]_{3\cdot 3d} \\ [0]_{3\cdot 2} & B_2 & [0]_{3\cdot 2} & [0]_{3\cdot 2d} & [0]_{3\cdot 3d} \\ [0]_{3\cdot 2} & [0]_{3\cdot 3} & B_3 & [0]_{3\cdot 2d} & [0]_{3\cdot 3d} \\ [0]_{3\cdot 2} & [0]_{3\cdot 3} & B_1 & [0]_{3\cdot 2d} & [0]_{3\cdot 3d} \\ [0]_{3k\cdot 2} & [0]_{3k\cdot 3} & B_4^{(k)} & [0]_{3k\cdot 2d} & B_2^{(k)}\delta_{kd} \\ [0]_{3d\cdot 2} & [0]_{3d\cdot 3} & [0]_{3d\cdot 2} & B_1^{(d)} & B_5^{(d)} \end{bmatrix}, \tag{21}$$

where $k = 1, 2, \ldots, N-1$, $d = 1, 2, \ldots, D$, and

$$B_1 = \begin{bmatrix} N_i & 0 \\ 0 & N_i \\ 0 & 0 \end{bmatrix}, \tag{22}$$

$$B_2 = \begin{bmatrix} -N_{xi} & -P_{xi} & -H_{xi} \\ -N_{yi} & -P_{yi} & -H_{yi} \\ 0 & 0 & 0 \end{bmatrix}, \tag{23}$$

$$B_3 = \begin{bmatrix} -\Lambda_{11}N_i & -\Lambda_{12}N_i \\ -\Lambda_{21}N_i & -\Lambda_{22}N_i \end{bmatrix}, \tag{24}$$

$$B_4 = \begin{bmatrix} a_{11}^{(k)}N_i & a_{12}^{(k)}N_i \\ a_{21}^{(k)}N_i & a_{22}^{(k)}N_i \\ 0 & 0 \end{bmatrix}. \tag{25}$$

3.3. Time integration

Equation of motion for dynamic behavior is given as

$$M\{\ddot{a}\}_{n+1} + C\{\dot{a}\}_{n+1} + K\{a\}_{n+1} = \{F\}_{n+1}, \tag{26}$$

where M, K, and C are the mass matrix, the stiffness matrix, and the damping matrix. $\{a\}$ is nodal displacement vector. F is external force. In the present study, damping term is neglected.

To solve the matrix equations of motion, the Newmark method (Sekine et al., 1998) is employed. This method is very popular and guarantees reliable solution. The Newmark scheme algorithm is given by

$$\{a\}_{n+1} = \{a\}_n + \Delta t\{\dot{a}\}_n + \left(\tfrac{1}{2} - \beta\right)\Delta t^2\{\ddot{a}\}_n + \beta\Delta t^2\{\ddot{a}\}_{n+1}, \tag{27}$$

$$\{\dot{a}\}_{n+1} = \{\dot{a}\}_n + (1-\gamma)\Delta t\{\ddot{a}\}_n + \gamma\Delta t\{\ddot{a}\}_{n+1}, \tag{28}$$

where Δt represents time step between t_{n+1} and t_n. The coefficients β and γ are parameters, which can be determined to obtain the integration accuracy and stability. The values of $\beta = 0.5$ and $\gamma = 0.7$ are picked up in the present study.

Substituting Eqs. (27) and (28) into (26), the matrix form of Eq. (26) can be written as

$$\widetilde{K}\{\ddot{a}\}_{n+1} = \widetilde{F}_{n+1}. \tag{29}$$

From Eq. (29), acceleration in the next step is obtained by calculating inverse of matrix $\widetilde{K}$. As this algorithm is repeated, time response of the delaminated plate structure can be obtained.

3.4. Time integration for considering dynamic contact algorithm

Unilateral contact algorithm is applied so that the time response may not violate the contact constraints. Dynamic equation of motion with contact algorithm can be expressed as follows:

$$M\{\ddot{a}\} + C\{\dot{a}\} + K\{a\} + G^{\mathrm{T}}\{\lambda\} = F, \tag{30}$$

$$G\{a\} = \delta^{w^{\mathrm{d}}}, \tag{31}$$

where G is the contact constraint matrix and $\delta^{w^{\mathrm{d}}}$ is the gap between upper layer and lower layer at the delamination interface.

Substituting Eqs. (27) and (28) into (30) and (31), equilibrium equations are reduced to the following matrix form:

$$\begin{bmatrix} \widehat{K} & G^{\mathrm{T}} \\ G & 0 \end{bmatrix} \begin{Bmatrix} a_{n+1} \\ \lambda_{n+1} \end{Bmatrix} = \begin{Bmatrix} R_{n+1} \\ \delta^{w^{\mathrm{d}}} \end{Bmatrix}, \tag{32}$$

where

$$\widehat{K} = \frac{2M}{\Delta t^2} + K, \qquad R_{n+1} = F_{n+1} + M\{\ddot{a}\}_n + \frac{2M}{\Delta t^2\beta}\left[\{a\}_n + \Delta t\{\dot{a}\}_n + \frac{\Delta t^2}{2}(1-2\beta)\{\ddot{a}\}_n\right]. \tag{33}$$

This algorithm is executed in the following manner. First, the nodal displacements which describe the relative motion of delaminations are constrained. Second, the reaction force and relative displacement of the delamination zone are checked. If the reaction force is positive or the relative displacement is negative, this contact algorithm is applied repeatedly until these contact conditions are satisfied. This scheme for satisfying contact constraints is applied in each time step.

In the delaminated zone, when the relative displacement was positive, the contact force was zero. That is, the time response is governed by Eq. (30). On the contrary, if the relative displacement was negative, contact force was imposed by Eq. (31). The behavior of composite plate with delaminations is predicted by using Lagrange multipliers to prevent penetration violation between delaminated layers.

4. Numerical examples

To assess the dynamic performance and the validity of the developed finite element of the present study, eigenvalue problem and time response problem for laminated composite plate with multiple and arbitrary shape delaminations are considered. Some of the results of the present theory are compared to the experiment results (Shen and Grady, 1992). In the circular and elliptic delamination cases, the variation of buckling loads is investigated as a function of the geometric size. Fig. 4 shows the mesh configuration of circular and elliptic delaminations. This simulation result can be baseline data for monitoring the health of laminated composite plates with arbitrary shaped multiple delaminations at any locations. For a multiple delamination case, a parametric study is performed. The results give the strength prediction of composite structures with multiple delaminations. To understand the dynamic responses with multiple delaminations in arbitrary position, Newmark scheme considering contact between interfaces is employed.

4.1. Eigenvalue problems

For the numerical evaluation of the performance of the proposed model, cantilever composite plates with center delamination are considered. The stacking sequence of the delaminated composite is $[(0/90)_2]_s$ and the thickness of plate is 1.016 mm. The plate has length $a = 127$ mm, and width $b = 12.7$ mm. The density is 1477 kg/m^2. The material properties of the numerical examples are given in the Table 1. In the present numerical examples, 18×4 mesh configuration is used for all computations. As shown in Fig. 5

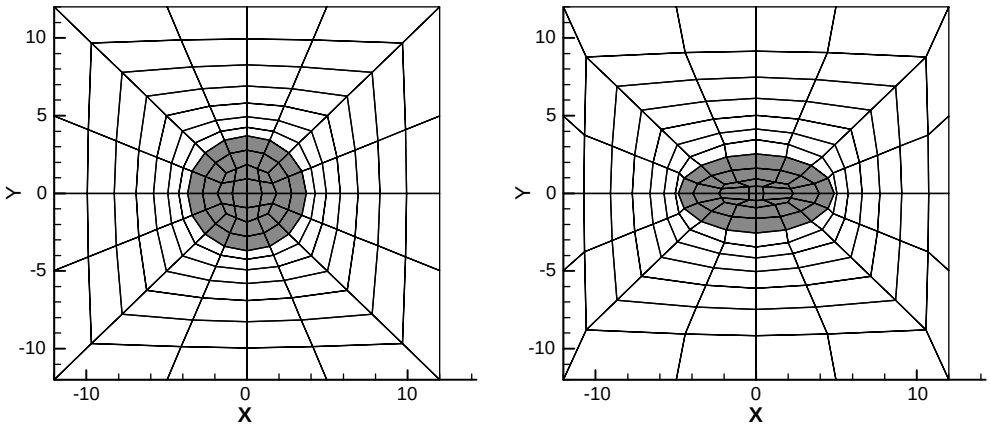

Fig. 4. Mesh configuration of the composite plate with a circular and elliptic delamination in center position. (Shaded areas indicate the circular and elliptic delamination zone, respectively.)

Table 1
Material properties

Graphite-epoxy layer
$E_1 = 1.344 \times 10^5$ MPa
$E_2 = E_3 = 1.034 \times 10^4$ MPa
$G_{12} = G_{13} = 4.999 \times 10^3$ MPa
$G_{23} = 1.999 \times 10^3$ MPa
$v = 0.33$

and Table 2, first, second, and third bending natural frequencies are predicted very accurately by the present finite element, better than Chattopadhyay et al. (2000) did. First bending natural frequency is higher than those of the experiment results (Shen and Grady, 1992). As the size of delaminated zone increases, the natural frequency is decreased. Second bending natural frequency occurs in accordance with NASTRAN solution. As the delamination length increases, the third bending natural frequency is dramatically decreased, much more than the first and second frequencies. The result of HOT of Fig. 5 was obtained from Chattopadhyay et al. (2000). The mode shapes of the above composite with delamination are shown in Fig. 6.

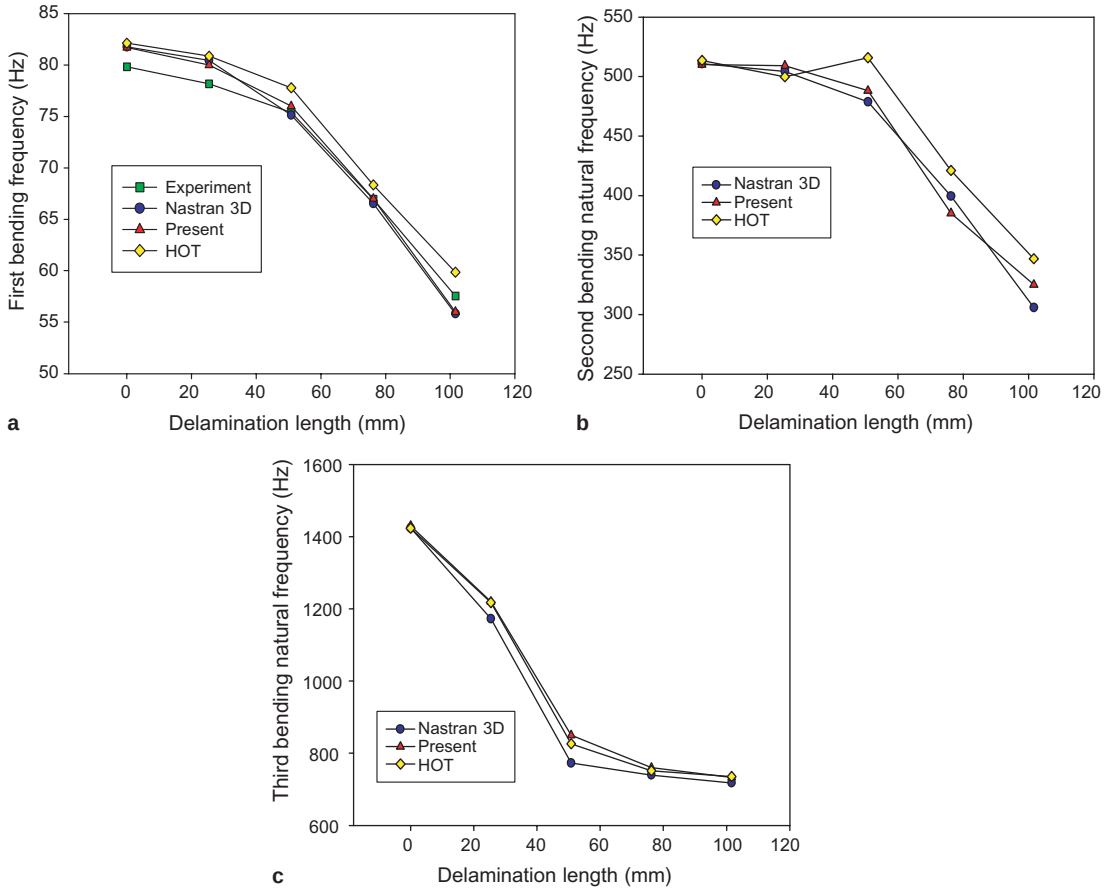

Fig. 5. First (a), second (b) and third (c) bending frequencies comparison between present and other results (Chattopadhyay et al., 2000).

Table 2
Bending frequency comparison

	Delamination length [mm]	Experiment[a] [Hz]	Nastran[a] 3D (element) [Hz]	HOT[a] [Hz]	Present theory [Hz]
First bending frequency	0	79.83	81.75	82.1	81.7
	25.4	78.16	80.429	80.8	80.2
	50.8	75.37	75.136	77.7	76.1
	76.2	66.95	66.531	68.3	67.2
	101.6	57.54	55.809	59.8	56.1
Second bending frequency	0	Null	510.7	513.4	510.1
	25.4		504.1	499.6	509.2
	50.8		478.6	515.7	488.1
	76.2		399.3	420.8	385.7
	101.6		305.7	346.7	325.4
Third bending frequency	0	Null	1423.8	1432.4	1430
	25.4		1172.8	1217.5	1220
	50.8		772.5	826.2	850
	76.2		739.6	751.3	760
	101.6		717.9	735.5	731

[a] (Chattopadhyay et al., 2000).

The mode shapes offer information on the position and shape of the delaminations. First and second bending modes are shown in Fig. 6(a) and (b), respectively. The first and second twisting modes are shown in Fig. 6(c) and (d), respectively. The third bending mode appears with two nodal lines as shown in Fig. 6(e).

For the multiple delamination case, the configurations of the multiple delaminations are shown in Fig. 7. Total of eight layers piled up. Number 1 represents the bottom interface, numbers 2, 3, and 4 locates above 1. This graph shows the natural frequency with the variation of the delamination positions. As shown in Fig. 8(a), the first natural frequency was decreased slightly, when the delamination is located near bottom. In Fig. 8(b), the second natural frequency was decreased dramatically, as the delamination approached the center. As the multiple delaminations approached the center, the plate became the more flexible. Fig. 8(c) shows the third natural frequency. The Fig. 8(c) shows that the frequency compared to that of the undelaminated case. The frequency predicted by the present model is always in the lower side. Fig. 8(d) shows the fourth natural frequency. The frequency of the fourth mode compared to that of the undelaminated case was significantly lower.

In the circular and elliptic delamination cases, the eigenvalue problem was analyzed using a clamped five-ply [0/90/0/90/0] composite plate model. The dimensions of the plate were length/width ratio = 1, and thickness length /thickness ratio was equal to 118. A circular delamination size was 30% of the whole composite plate. From Fig. 9 and Table 3, it can be seen that the frequency changes according to delamination shape effect. The Fig. 10 shows geometry of composite plate with elliptic delamination. The delamination size affected the higher frequencies much more than the lower frequencies. The position information of arbitrary and multiple delaminations of a global structure can be obtained accurately because the present finite element is reliable for arbitrary shape of delaminations.

4.2. Dynamic responses

Deflections of the composite plates with rectangular, circular (length ratio $r = 1$), and elliptic (length ratio $r = 1.9091$) delaminations were obtained by time integration analysis, considering the constraint of contact.

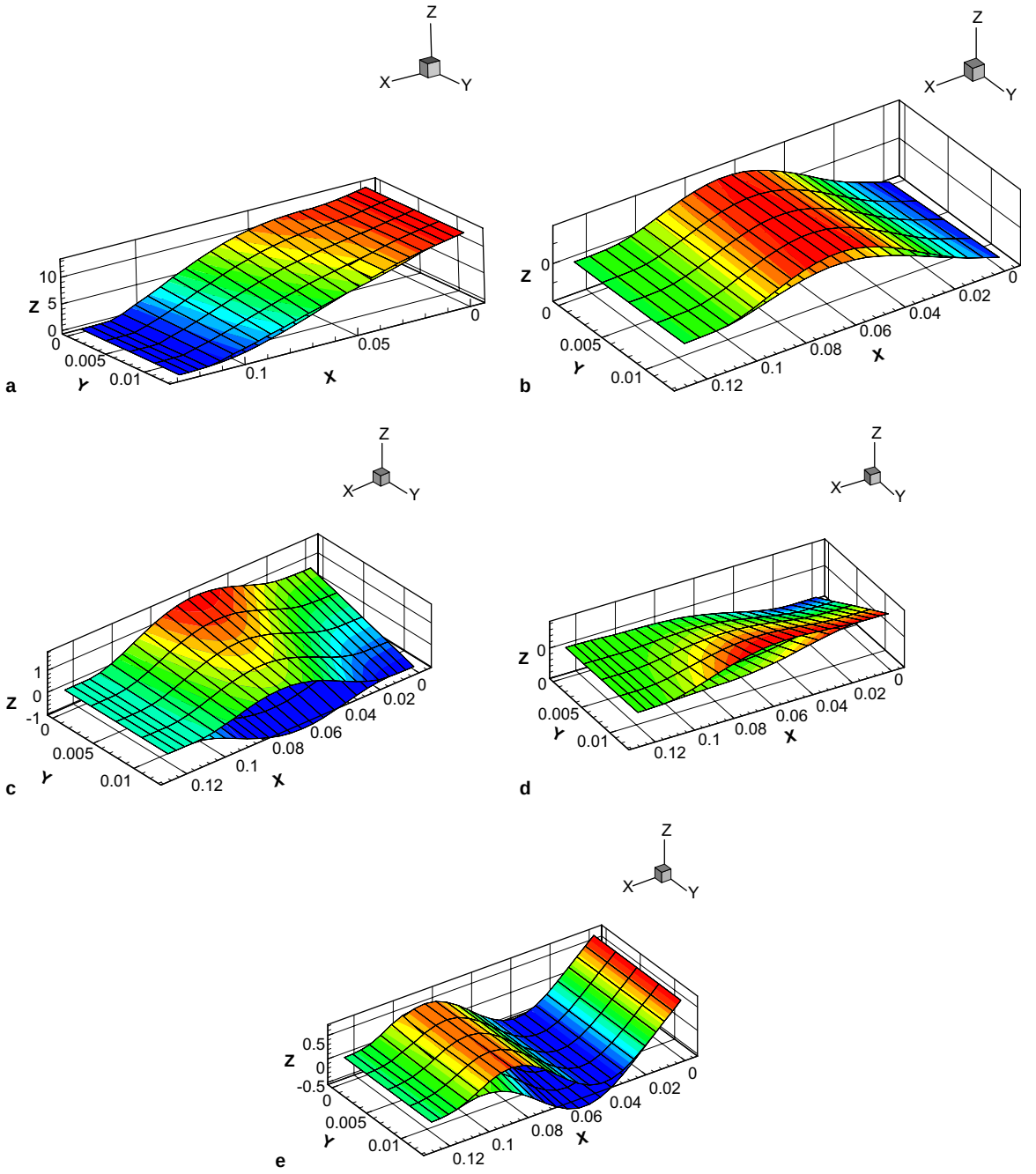

Fig. 6. First bending (a), second bending (b), first twisting (c), second twisting (d) and third bending (e) mode shapes.

Clamped square plate with [0/90/0/90/0] layup is considered. The material properties for this case are given in Table 1. In the rectangular-shaped delamination case, the geometric configuration is given as length/width ratio = 10 and length/thickness ratio = 125. Flow chart of contact algorithm in time

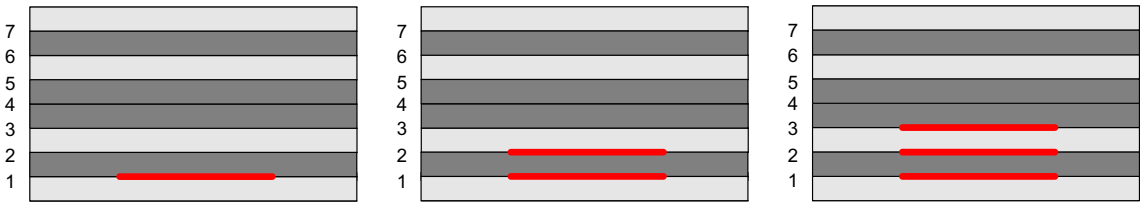

Fig. 7. Delamination position at the interfaces between layers of composite plate.

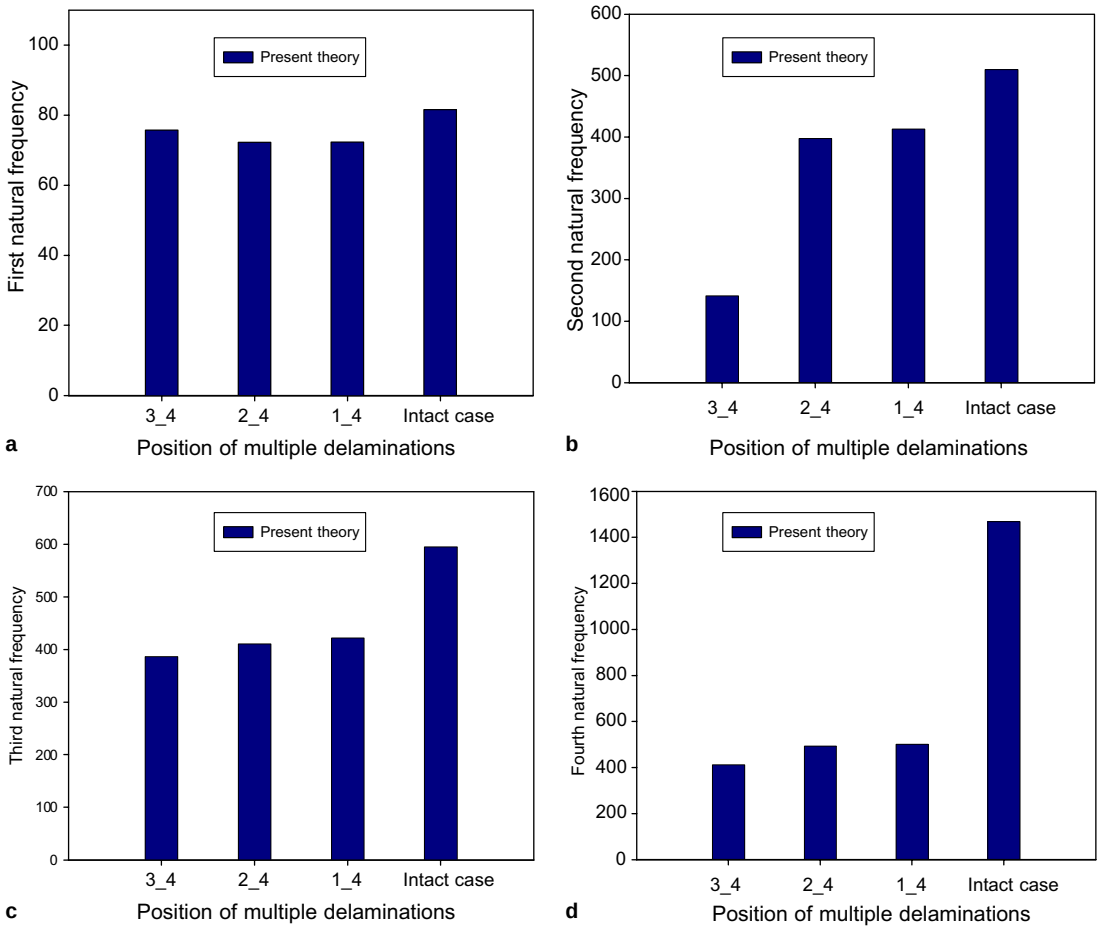

Fig. 8. First (a), second (b), third (c) and fourth (d) natural frequency with the variation of delamination positions.

integration is given in Fig. 11. To visualize delamination zone response behaviors more distinctly, the relative transverse displacements of rectangular delaminated zone shown in Fig. 13 are magnified by 5 times. Delamination zone size is set to 50% of the whole plate in this case. Fig. 12(a) shows the vertical displacement of rectangular-shaped delamination zone without considering penetration violation. As the time step increases, the penetration violation in the delamination zone appears.

The time responses with contact constraints are compared to those without constraints. The higher modes appear more distinctly in the case without considering contact conditions while in the case of considering contact the higher frequency modes do not appear clearly in the global motion because higher modes are strictly constrained to satisfy unilateral contact conditions. Even though the frequencies of the model with contact constraints are quite close to the one without contact constraints, the time responses

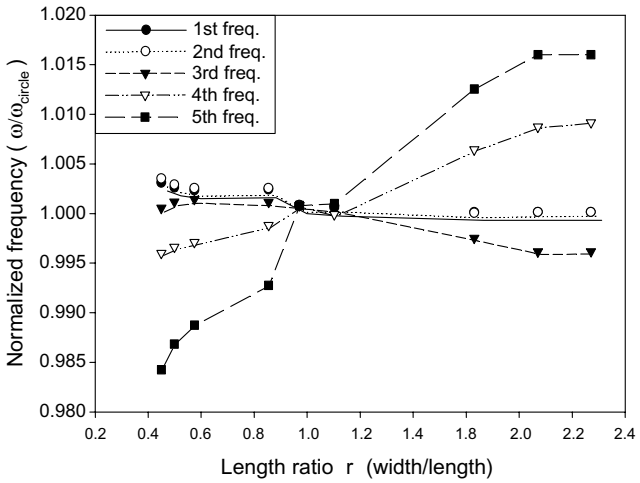

Fig. 9. Normalized frequency vs. delamination length ratio.

Table 3
Frequency according to the change of delamination length ratio

a/*b* (width/length)	First frequency [Hz]	Second frequency [Hz]	Third frequency [Hz]	Fourth frequency [Hz]	Fifth frequency [Hz]
0.4737	0.24416	0.32443	1.01769	1.5455	1.6562
0.7778	0.24407	0.32427	1.01803	1.5465	1.6601
1	0.24388	0.32399	1.01783	1.5492	1.6700
1.6667	0.24379	0.32387	1.01616	1.5535	1.6797
1.9091	0.24378	0.32388	1.01546	1.5556	1.6826

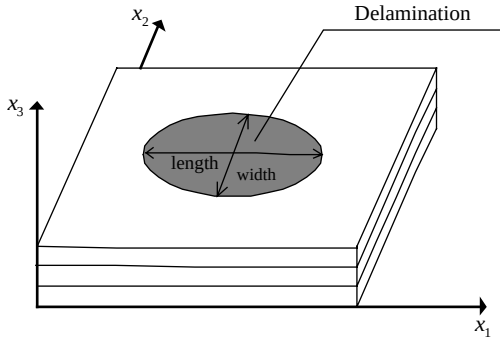

Fig. 10. The geometry of composite plate with elliptic delamination.

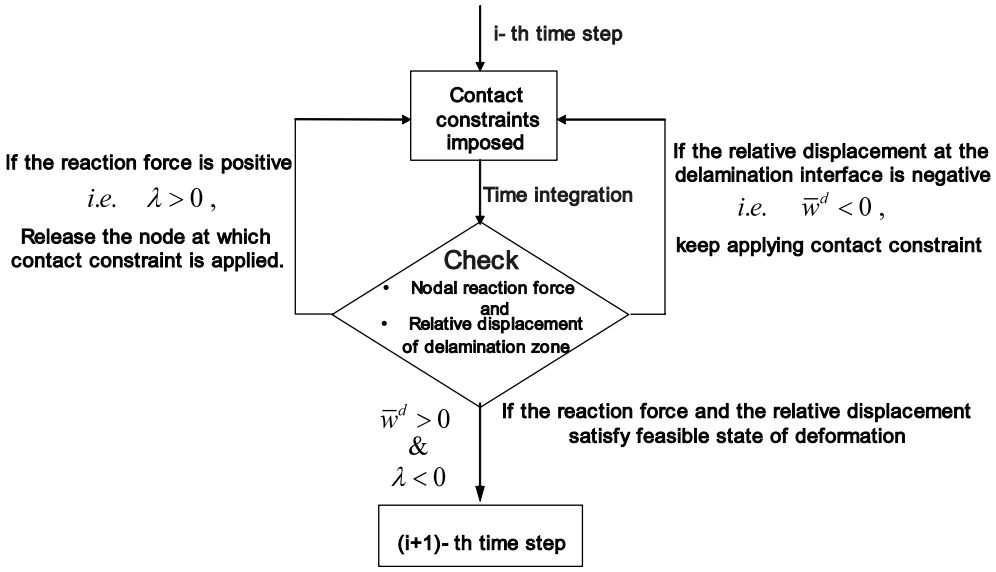

Fig. 11. Flow chart of contact algorithm in time integration.

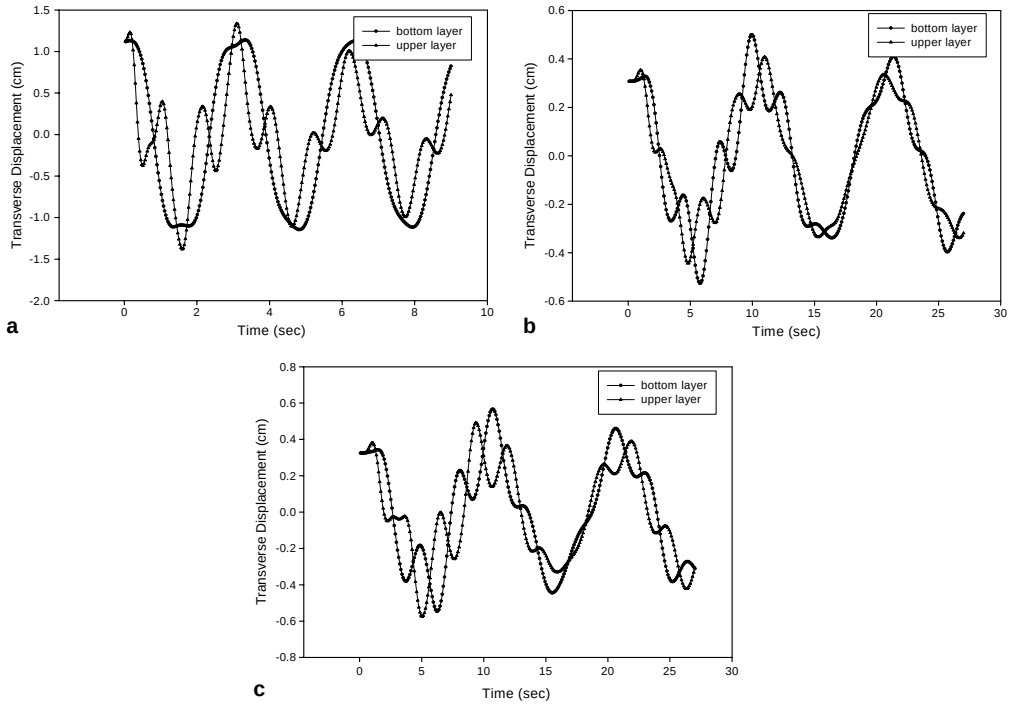

Fig. 12. (a) Dynamic response of the laminated plate with the rectangular delaminated zone without contact constraint. (b) Dynamic response of the laminated plate with the circular delaminated zone without contact constraint. (c) Dynamic response of the laminated plate with the elliptic delaminated zone without contact constraint.

are significantly different from each other. In the situation of delamination zone closed, the response considering contact conditions show mostly fundamental mode of time response. And when delamination zones become open, high frequency modes and contact behavior appear.

As shown from Figs. 13–15, the time response of the plate with a circular delamination is quite different from that with the rectangular delamination but the response with elliptic delamination is qualitatively quite similar to the case of circular delamination. Fig. 13(a) shows the vertical displacement of the plate with a rectangular delamination zone when the contact constraint is considered. This figure shows that the delamination interface opens when the plate is bent downward. Similar to Fig. 13(a), Fig. 13(b) and (c) represent the vertical displacement with nodes of number 1, 2 and number 1, 2, and 3 positions, which is depicted in Fig. 7. As the number of delamination interfaces through the thickness increases, the delamination opening amplitude decreases.

In circular and elliptic delamination problem, the transverse displacements in the delamination zone are magnified by 3 times and they are shown in Figs. 14 and 15. Elliptic delamination length ratio r is 1.9091. Comparing Fig. 13(a) with Fig. 14(a), the opening amplitude of rectangular delamination case is larger than that of the circular delamination case. From Figs. 13–15, the circular and elliptic delamination interface opening is observed more frequently than the rectangular delamination case.

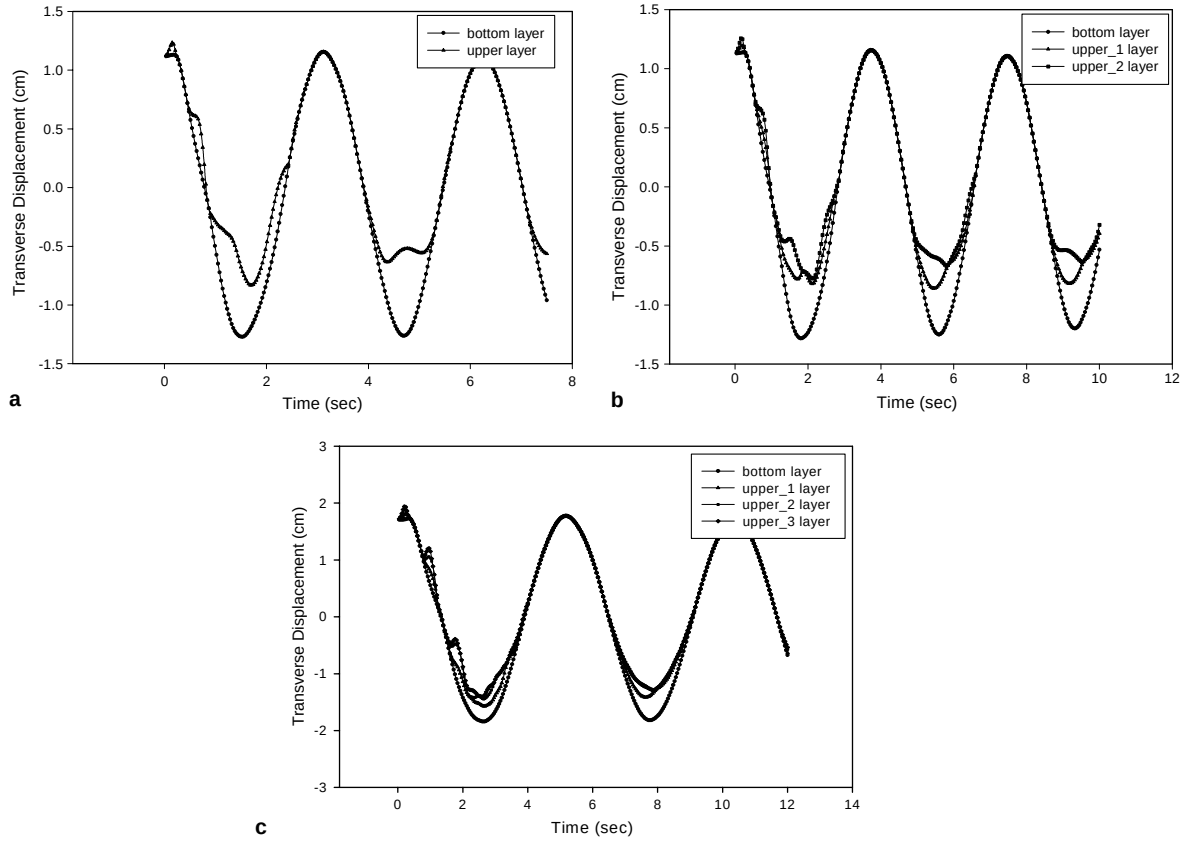

Fig. 13. (a) Dynamic response of the laminated plate with one rectangular delamination. (b) Dynamic response of the composite plate with two rectangular delaminations. (c) Dynamic response of the composite plate with three rectangular delaminations.

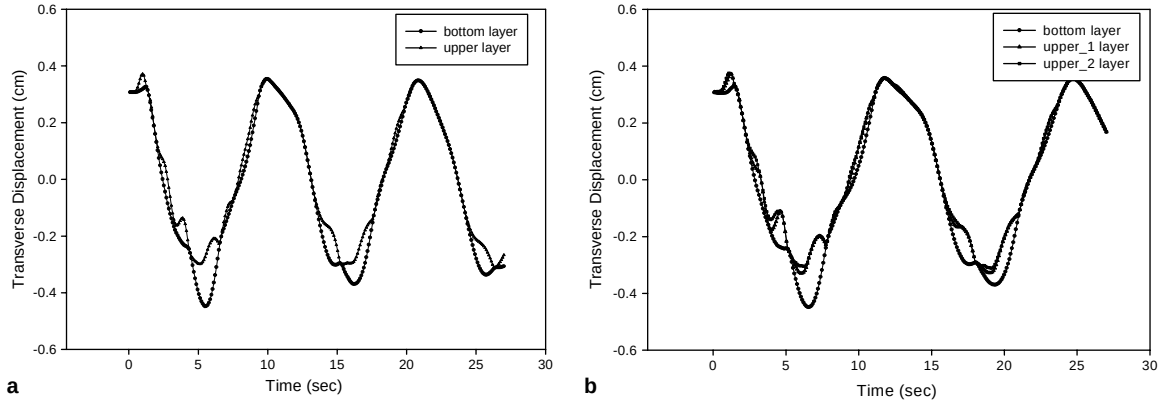

Fig. 14. Dynamic response of the composite plate with one (a) and two (b) circular delaminations.

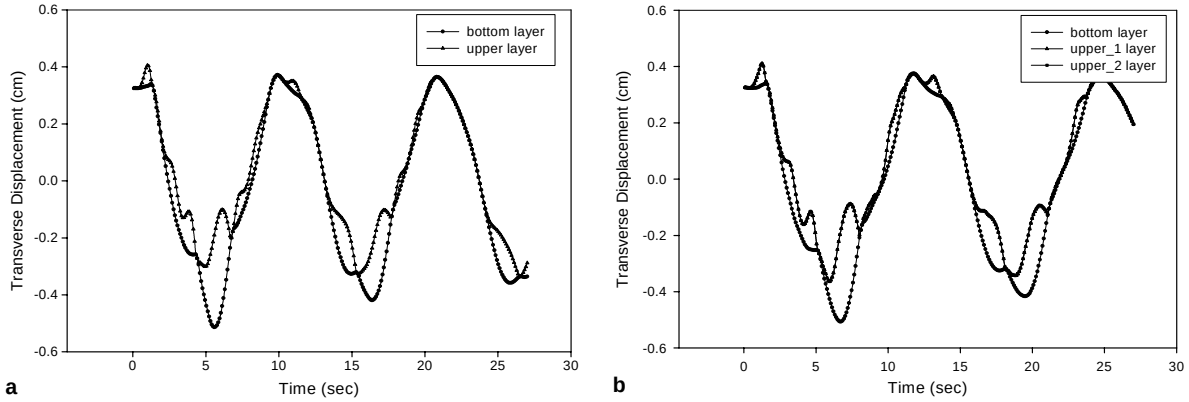

Fig. 15. Dynamic response of the case with one (a) and two (b) elliptic delaminations.

5. Conclusions

In the present study, a finite element based on a higher-order zigzag theory with multiple delaminations was developed to analyze the dynamic behavior of a structure with multiple delaminations. By imposing transverse shear stress free condition of the top and bottom surfaces and stress interface continuity conditions between the layers with delaminations, layer-dependent displacement variables were eliminated. Final displacement fields of the undelaminated zone have only reference primary variables. In the delaminated zone, the minimal number of degrees-of-freedom is still retained. Thus, this theory can be applied to the problems with many thick layers and multiple delaminations.

Through the eigenvalue problem and time integration analysis of composite plates with multiple delaminations, it is observed that the natural frequencies predicted by the present EHOPTWD are in good agreement with experiment data, HOT and NASTRAN-3D solutions. The present finite element based on the zigzag higher-order theory demonstrated accurate predictions of natural frequencies and mode shapes for various types of delaminations in the moderate thick plate range.

For the time integration scheme, to prevent the penetration problem in the delamination zone, Lagrange multiplier method was applied. The time response considering unilateral contact constraint through

Lagrange multipliers was performed by Newmark scheme. The present four-node zigzag finite element which retains the minimal degrees of freedom for composite plate with multiple delaminations showed its applicability and effectiveness in dynamic analysis.

References

Batoz, J.L., Tahar, M.B., 1982. Evaluation of a new quadrilateral thin plate bending element. International Journal for Numerical Methods in Engineering 18, 1655–1677.

Chattopadhyay, A., Gu, H., 1994. New higher order theory in modeling delamination buckling of composite laminates. AIAA Journal 32, 1709–1716.

Chattopadhyay, A., Dragomir-Daescu, D., Gu, H., 1999. Dynamics of delaminated smart composite cross-ply beams. Smart Materials and Structures 8, 92–99.

Chattopadhyay, A., Radu, A.G., Dragomir-Daescu, D., 2000. A higher order plate theory for dynamic stability analysis of delaminated composite plates. Computational Mechanics 26, 302–308.

Cheng, Z.-q., Jemah, A.K., Williams, F.W., 1996. Theory for multilayered anisotropic plates with weakened interfaces. Journal of Applied Mechanics 63, 1019–1026.

Cheung, Y.K., Zhang, Y.X., Wanji, C., 2000. The application of a refined non-conforming quadrilateral plate bending element in thin plate vibration and stability analysis. Finite Element in Analysis and Design 34, 175–191.

Cho, M., Kim, J.H., 1996. Postprocess method using displacement field of higher order laminated composite plate theory. AIAA Journal 34 (2), 362–368.

Cho, M., Kim, J.S., 1997. Bifurcation buckling analysis of delaminated composites using global–local approach. AIAA Journal 35 (10), 1673–1676.

Cho, M., Kim, J.S., 2001. Higher order zig-zag theory of laminated composites with multiple delaminations. Journal of Applied Mechanics 68, 869–877.

Cho, M., Lee, S.G., 1998. Global/local analysis of laminated composites with multiple delaminations of various shapes. In: Proceedings of the AIAA/ASME/ASCE/AHS/ASC 39th Structures, Structural Dynamics and Materials Conference, Long Beach, CA, AIAA, Reston, VA. pp. 76–86.

Cho, M., Parmerter, R.R., 1992. An efficient higher-order plate theory for laminated composites. Composite Structures 20, 113–123.

Cho, M., Parmerter, R.R., 1993. Efficient higher order composite plate theory for general lamination configurations. AIAA Journal 31 (7), 1299–1306.

Di Sciuva, M., 1986. Bending, vibration and buckling of simply supported thick multilayered orthotropic plates: an evaluation of a new displacement model. Journal of Sound and Vibration 105, 425–442.

Di Sciuva, M., 1997. Geometrically nonlinear theory of multilayered plates with interlayer slips. AIAA Journal 35, 1753–1759.

Gummadi, L.N.B., Hanagud, S., 1995. Vibration characteristics of beams with multiple delaminations. In: Proceedings of the AIAA/ASME/-ASCE/AHS/ASC 36th Structures, Structural Dynamics and Materials Conference, New Orleans, LA, AIAA, Reston, VA. pp. 140–150.

Islam, A.S., Craig, K.C., 1994. Damage detection in composite structures using piezoelectric materials. Smart Materials and Structures 3, 318–328.

Kapania, R.K., Raciti, S., 1989. Recent advanced in analysis of laminated beams and plates. AIAA Journal 27, 923–946.

Kim, J.S., Cho, M., 1999. Postbuckling of delaminated composites under compressive loads using global–local approach. AIAA Journal 37 (6), 774–778.

Kim, J.S., Cho, M., 2002. Buckling analysis for delaminated composites using plate bending elements based on higher-order zig-zag theory. International Journal for Numerical Methods in Engineering 55 (1), 1323–1343.

Kim, J.S., Cho, M., 2003. Efficient higher order shell theory for laminated composites with multiple delaminations. AIAA Journal 41 (5), 941–950.

Lee, J., Gurdal, Z., Griffin, O.H., 1993. Layer-wise approach for the bifurcation problem in laminated composites with delaminations. AIAA Journal 31, 331–338.

Lo, K., Christensen, R.M., Wu, E.M., 1977. A higher-order theory of plate deformation, Part 2: Laminated plates. Journal of Applied Mechanics 44, 669–676.

Noor, A.K., Burton, W.S., 1989. Assessment of shear deformation theories for multilayered composite plates. Applied Mechanics Reviews 42, 1–13.

Ramkumar, R.L., Chen, P.C., Pipes, R.B., 1983. Low-velocity impact response of laminated plates. AIAA Journal 21, 1448.

Reddy, J.N., 1987. A generalization of two-dimensional theories of laminated plates. Communications in Numerical Methods in Engineering 3, 173–180.

Reddy, J.N., Robbins Jr., D.H., 1994. Theories and computational models for composite laminates. Applied Mechanics Reviews 47, 147–169.

Seeley, C.E., Chattopadhyay, A., 1999. Modeling of adaptive composites including debonding. International Journal of Solids and Structures 36, 1823–1843.

Sekine, H., Hu, N., Fukunaga, H., Natsume, T., 1998. Low-velocity impact response of composite laminates with a delamination. Mechanics of Composite Materials and Structures 5, 257–278.

Shen, M.-H.H., Grady, J.E., 1992. Free vibration of delaminated beams. AIAA Journal 30, 1361–1370.

Specht, B., 1988. Modified shape functions for the three-node plate bending element passing the patch test. International Journal for Numerical Methods in Engineering 26, 705–715.

Thomas, J.R.H., Robert, L. Taylor, Jerome, L. Sackman, Alain, Curnier, Worsak, Kanoknukulchai, 1976. A finite element method for a class of contact-impact problems. Computer Methods in Applied Mechanics and Engineering 8, 249–276.

Todd, O.W., Frank, L.A., 1998. A dynamic model for laminated plates with delaminations. International Journal of Solids and Structures 35, 83–106.

Wang, J.T.S., Lin, C.C., 1995. Vibration of beam-plates having multiple delaminations. In: Proceedings of the AIAA/ASME/ASCE/AHS/ASC 36th Structures, Structural Dynamics and Materials Conference, New Orleans, LA, AIAA, Reston, VA. pp. 3126–3133.

Wang, J.T.S., Liu, Y.Y., Gibby, J.A., 1982. Vibrations of split beams. Journal of Sound and Vibration 84, 491–502.

Wanji, C., Cheung, Y.K., 1997. Refined non-conforming quadrilateral thin plate bending element. International Journal for Numerical Methods in Engineering 40, 3919–3935.